



Genetic and pharmacological inhibition of acid ceramidase prevents asymmetric cell division by neosis^S

Shai White-Gilbertson, Ping Lu, James S. Norris, and Christina Voelkel-Johnson¹

Department of Microbiology and Immunology, Medical University of South Carolina, Charleston, SC 29425

ORCID ID: 0000-0001-6909-6678 (C.V.J.)

Abstract Radiation treatment failure or relapse after initial response to chemotherapy presents significant clinical challenges in cancer patients. Escape from initial courses of treatment can involve reactivation of embryonic developmental stages, with the formation of polynuclear giant cancer cells (PGCCs). This strategy of dedifferentiation can insulate cancer cells from a variety of treatments and allows a residual subpopulation to reestablish tumors after treatment. Using radiation or docetaxel chemotherapy, we generated PGCCs from prostate cancer cells. Here, we show that expression of acid ceramidase (ASAHI), an enzyme in the sphingolipid pathway linked to therapy resistance and poor outcomes, is elevated in PGCCs. Targeting ASAHI with shRNA or treatment with the ASAHI inhibitor, LCL-521, did not impair the formation of PGCCs, but prevented the formation of PGCC progeny that arise through an asymmetric cell division called neosis. Similar results were obtained in lung cancer cells that had been exposed to radiation or cisplatin chemotherapy as stressors. In summary, our data suggest that endoreplication occurs independent of ASAHI while neosis is ASAHI-dependent in both prostate and lung cancer cells. Because ASAHI knockout is embryonic lethal but not deleterious to adult animals, targeting this enzyme has the potential to be highly specific to cells undergoing the dedifferentiation process to escape cancer treatments. **Pharmacological inhibition of ASAHI is a potentially powerful strategy to eliminate cells that could otherwise serve as seed populations for recurrence.**—White-Gilbertson, S., P. Lu, J. S. Norris, and C. Voelkel-Johnson. **Genetic and pharmacological inhibition of acid ceramidase prevents asymmetric cell division by neosis.** *J. Lipid Res.* 2019. 60: 1225–1235.

Supplementary key words apoptosis • cancer • sphingolipids • ceramide • drug therapy • lipidomics • polynuclear giant cancer cells

The majority of cancer therapies aim at disrupting the mitotic process, which in cancer, by definition, is both deregulated and overactive. Treatments such as ionizing radiation and chemotherapy decommission various pieces of the mitotic machinery, leading to well-known side effects in patients as healthy mitotic cells are invariably impacted. A less understood and unintended effect on the cancer cells is endoreplication (also known as endoreduplication), a process during which genetic material is copied in the absence of mitotic division, resulting in the accumulation of multiple nuclei in a single cell to create polynuclear giant cancer cells (PGCCs) (1, 2). This functionality requires remarkable dedifferentiation and may only occur in a minority of treated cancer cells. Niu and colleagues have elegantly described these treatment-resistant cancer cells as being the somatic equivalent of blastomeres, which comprise the 2- to 16-cell stage of embryogenesis (3, 4). As PGCCs are no longer tied to mitosis, they can survive radiation and/or chemotherapy and have the potential to form the seed population for cancer relapse (5–9). Once treatment stress is relieved, PGCCs undergo a form of asymmetric cell division known as neosis, which is akin to budding and circumvents mitotic catastrophe (10–12). A major challenge in cancer research is to understand how neosis can be prevented in PGCCs.

In recent years, the enzyme, acid ceramidase (ASAHI), has increasingly gained attention as playing a role in therapy resistance and tumor aggressiveness (13–16). ASAHI is a lysosomal enzyme in the sphingolipid metabolic pathway that hydrolyzes the pro-apoptotic sphingolipid, ceramide, to generate sphingosine. ASAHI has recently been found to be critical in the survival of cancer stem cells (CSCs) in

This project was supported by National Cancer Institute Grant P01 CA203628. The content is solely the responsibility of the authors and does not necessarily represent the official views of the National Institutes of Health. The Medical University of South Carolina Foundation for Research has licensed LCL-521 to SphingoGene, Inc. (J.S.N.). J.S.N. is the Chairman of the Board and Interim CEO of SphingoGene, Charleston, SC. The remaining authors declare no competing financial interests.

Manuscript received 3 January 2019 and in revised form 27 March 2019.

Published, JLR Papers in Press, April 15, 2019

DOI <https://doi.org/10.1194/jlr.M092247>

Copyright © 2019 White-Gilbertson et al. Published under exclusive license by The American Society for Biochemistry and Molecular Biology, Inc.

This article is available online at <http://www.jlr.org>

Abbreviations: ALDH, aldehyde dehydrogenase; ASAHI, acid ceramidase; CDK1, cyclin-dependent kinase 1; CSC, cancer stem cell; DES1, dihydroceramide desaturase; FSC, forward scatter count; NSCLC, non-small cell lung cancer; PARP, poly (ADP-ribose) polymerase; PGCC, polynuclear giant cancer cell; SCC, side scatter count; SK, sphingosine kinase; SIP, sphingosine 1-phosphate.

¹To whom correspondence should be addressed.

e-mail: johnsovc@musc.edu

^SThe online version of this article (available at <http://www.jlr.org>) contains a supplement.

melanoma and glioblastoma (17, 18). Previous work from our group has shown that ASAH1 contributes to radiation therapy failure in prostate cancer and that pharmacological inhibition of ASAH1 in a preclinical model of prostate cancer prevented relapse after radiation treatment (19). However, the underlying mechanism by which ASAH1 inhibition resulted in apparent cures remained elusive.

Cancer cells that survive initial treatment and drive recurrence are thought to be generally more fit, have increased drug efflux capacity, or to be senescent, but the novel idea of dedifferentiation as an escape strategy is also gaining support (4, 20, 21). Studies with knockout mice have shown that deletion of ASAH1 is embryonic lethal at the 2- to 4-cell stage, yet conditional knockout mice did not exhibit defects, with the exception of reduced fertility in females (22, 23). We hypothesized that ASAH1 plays a parallel role in the survival of embryonic cells at the blastomere stage and dedifferentiated PGCCs, prompting us to investigate the role of ASAH1 in this cancer cell subpopulation. Here, we report that neosis in PGCCs is critically dependent on ASAH1 expression and activity, which supports our hypothesis and provides a map for how to leverage these similarities.

MATERIALS AND METHODS

Cell culture, cell lines, generation of PGCCs

Sources of cell lines were as follows: PPC1 prostate adenocarcinoma cells were obtained from Dr. Dean Tang (Roswell Park Comprehensive Cancer Center, Buffalo, NY); A549 small cell lung cancer cells were a gift from Dr. Besim Ogretmen (Medical University of South Carolina, Charleston, SC); and SW620 colon carcinoma cells were purchased from the American Type Culture Collection (Rockville, MD). Cells were cultured in RPMI medium (PPC1) or DMEM (A549, SW620) (Cellgro, Manassas, VA) supplemented with 10% FBS (Hyclone, Logan, UT) and 1% antibiotic-antimycotic solution (Gibco, Grand Island, NY). Cells were maintained at 5% CO₂ in a humidified incubator and were periodically verified to be free of mycoplasma contamination with a MycoAlert PLUS kit (Lonza, Allendale, NJ).

To generate PPC1 cells expressing the ASAH1-driven GFP reporter plasmid, pcDNA3-GFP (plasmid #13031; Addgene) and pGL3-ASAH (a kind gift from Dr. Marion Sewer) containing the -2,740 to +1 ASAH1 promoter were digested with MluI/BamHI to remove the CMV and ASAH1 promoters (24). Following gel purification, the ASAH1 promoter was inserted into the MluI/BamHI sites of the GFP plasmid. PPC1 cells were transfected using Lipofectamine 2000 (Invitrogen, Carlsbad, CA) and selected in 600 µg/ml G418 (Cellgro).

SmartVector inducible human shRNA plasmids were purchased from Dharmacon (LaFayette, CO) (ASAH1 shRNA: V3SH11252-226369646, V3SH11252-230593210; nontargeting control: VSC11651). Lentiviral vectors were generated according to the manufacturer's instructions (Dharmacon trans-lentiviral packaging kits).

To generate PGCCs, cells were plated as described for each assay and treated with 5 nM docetaxel (Zydus Hospira Oncology, Lake Forest, IL), 30 µM cisplatin (a gift from Dr. Besim Ogretmen), or were irradiated in a ¹³⁷Cs γ-irradiator (J. L. Shepherd and Associates, San Fernando, CA) to the indicated dose. Cells were then allowed to undergo endoreplication until PGCCs could be visually confirmed to be the majority of the remaining adherent

cells, typically about 48 h. While the doses and timeframes for docetaxel were determined empirically, similar experimental approaches have previously been reported to be dose- and time-dependent phenomena after application of the drug (7). For radiation treatment, we confirmed that PGCC formation in response was also a simple dose- and time-dependent phenomenon by comparing the more experimentally convenient single dose of radiation to an equal fractionated dose, and confirmed that cell responses were similar (supplemental Fig. S1). LCL-521 was developed by and obtained from the Medical University of South Carolina Lipidomics Core facility (25). LCL-521 was dissolved to 50 mM in 100% ethanol and stored at -20°C for no longer than 3 months.

Flow cytometry

For quantification of PGCCs by size, cells were detached with 0.25% trypsin (Gibco), fixed in 4% formaldehyde (Thermo Scientific, Kalamazoo, MI) at 4°C for at least 30 min, washed with PBS (Mediatech, Manassas, VA), and resuspended in FACS buffer (PBS, 5% FBS, 0.5 M EDTA from EM Science, Gibbstown, NJ, and 0.8 mM sodium azide from Fisher Scientific, Fair Lawn, NJ). As a negative control, a polygon gate was used to describe the size of untreated PPC1 cells, and larger cells outside that gate were considered PGCCs. Alternatively, a histogram over a side-scatter x-axis was used to define PGCCs. For cell cycle analysis, cells were trypsinized and fixed by the dropwise addition of 100% ice-cold ethanol to a final concentration of 50%. Cells were fixed for 30 min at room temperature, spun down, and resuspended in 10 µg/ml RNase (Fisher Bioreagents, Fair Lawn, NJ) and 20 µg/ml propidium iodide (AnaSpec, Inc., Fremont, CA) for 20 min at room temperature. Cells were then washed with PBS twice and resuspended in FACS buffer. For all PGCC quantification assays, 10,000 events per sample were acquired on a BD LSRFortessa cell analyzer (BD Biosciences, San Jose, CA). Debris was gated out and the remaining cells (typically 8,500–9,500) were analyzed using FlowJo software (Tree Star Inc., San Diego, CA). For GFP-expressing PPC1 cells, an additional analysis comparing GFP signal between treatments was performed on the same gated populations.

For CD133 staining, PGCCs were prepared as above, harvested with Cell Stripper (Cellgro), pelleted, and resuspended in 400 µl of PBS, which was then split into two aliquots of 200 µl each for each sample. One aliquot was incubated with 1 µl of anti-CD133 conjugated to a PE fluorophore [Miltenyi Biotec, Cambridge, MA; #CD133/1(AC133)-PE] for 15 min on ice, and one was incubated without antibody. Samples were washed with PBS, resuspended in 3.7% formaldehyde for at least 20 min on ice, washed, resuspended in FACS buffer, and acquired on a BD LSRFortessa. Unstained samples were used to create a negative gate and stained samples overlaid using FlowJo software. Stained cells with signal exceeding the unstained cells were considered positive for CD133. SW620 cells were used as a positive control.

For aldehyde dehydrogenase (ALDH) activity analysis, cells were prepared according to manufacturer's instructions for the Aldefluor kit (Stemcell, Cambridge, MA). Briefly, cells were trypsinized, resuspended in assay buffer, and each sample split into two aliquots, both of which received substrate, but only one of which received aldehyde activity inhibitor (DEAB). Samples were incubated at 37°C for 40 min and FITC signal indicating aldehyde activity was quantified. DEAB(+)-containing samples were used to draw negative gates for each sample in FlowJo. The matching DEAB(-) sample was overlaid to quantify the percent of positive signal per sample compared with a self-negative control.

Western blotting

Cells were plated at 6×10^5 cells per 100 mm dish and allowed to adhere overnight. The next day, docetaxel (5 nM) or radiation

(8 Gy) was administered. After 48 h, medium containing floating cells was harvested and pelleted. Adherent cells were scraped into PBS and pelleted. Western blotting was performed as described previously (26). Primary antibodies (1:1,000) were ASAHI (BD Transduction Laboratories; #612302), dihydroceramide desaturase (DES1) (Abcam, Cambridge, MA; #ab167169), sphingosine kinase (SK)1 (Cell Signaling, Danvers, MA; #12071), cleaved poly (ADP-ribose) polymerase (PARP) (Cell Signaling; #9546), and GAPDH (Santa Cruz Biotechnology, Dallas, TX; #sc-32233). Secondary antibodies (1:5,000) were obtained from Santa Cruz Biotechnology (anti-mouse #sc-2005 and anti-rabbit #sc-2004).

Visual imaging

All images were captured with a Zeiss Axiovert 200 and minimally processed for clarity using standard PowerPoint tools. All images were taken with bright field settings with the exception of Fig. 1B, which includes an overlay to visualize nuclei, taken with a UV filter after incubating cells with 10 μ g/ml Hoechst dye (Acros Organics, Belgium) for 10 min.

Crystal violet staining and quantification

For chemotherapy-based assays, cells were plated 1.8×10^5 per well of a 6-well plate for PPC1 cells or 2×10^5 for A549 cells. For radiation-based assays, cells were plated onto 60 mm dishes. Cells were allowed to adhere overnight and treated as indicated the next day. In Fig. 4, LCL-521 was added immediately after adding docetaxel or radiation treatment. Medium and drug were refreshed every 2 days until new colonies emerged (between 3 and 6 days, with docetaxel-induced PGCCs recovering earlier than radiation-induced PGCCs). In Fig. 5, after the appearance of PGCCs, the cell layer was trypsinized, resuspended in approximately 10 ml of medium, and passed through a 20 micron filter (Pluriselect, San Diego, CA). Ten milliliters of PBS were then passed through the filter to wash the captured cells. The filter was inverted, placed onto a fresh 50 ml tube, and washed to release PGCCs. Cells were replated onto 60 mm dishes and allowed to adhere for at least 6 h before adding LCL-521 at the indicated concentrations. LCL-521 was refreshed every 2 days until new colonies emerged under control conditions. At the end of each assay, medium was removed, the cell layer washed with PBS, and ice-cold methanol (VWR, West Chester, PA) added to each well or dish for 20 min for fixation. The methanol was removed, the plates allowed to dry, and approximately 4 ml of a 0.05% crystal violet dye (Sigma, St. Louis, MO) were added to each plate for 20 min. The dye was then washed off with tap water and the plates dried prior to morphological analysis, crystal violet quantification, or colony counting. For quantification of data shown in Fig. 4, dye was released from the cells with 10% acetic acid (Fisher Scientific) and read in triplicate using a FLUOstar Optima plate reader (BMG Labtech, Cary, NC). In Fig. 5, each 60 mm plate was divided into sections and one section per sample was randomly chosen for evaluation. Colonies containing at least 15 cells were counted.

LC/MS analysis of sphingolipids

In Fig. 2, cells were plated at 6×10^5 cells per 100 mm plate and allowed to attach overnight. The next day, 5 nM of docetaxel were added to the medium or 8 Gy were administered. After 48 h, floating cells were harvested and collected by centrifugation. Adherent cells were scraped into PBS and pelleted. Cell pellets were delivered to the Medical University of South Carolina Lipidomics Core facility for analysis. Ceramide species [total ceramide, sphingosine, and sphingosine 1-phosphate (S1P)] were quantified by LC/MS as previously described (27). Normalization was performed using the total phosphate content within each submitted fraction. For analysis requiring only harvest of adherent cells, samples were normalized to total protein (if the cells had been

exposed to long-term treatment that could result in loss of cell number) or to cell number (if only baseline measurements or short-term drug exposure with negligible toxicity was involved) (supplemental figures).

Statistical methods

Student's *t*-test, with a two-sided α of 0.05 set as significant, was used for all comparisons between groups except for Fig. 1D, where a one-way ANOVA analysis was performed to compare three methods, with statistical significance set at $P = 0.05$. Each experiment shown was performed as at least three independent assays, typically run in triplicate each time. Throughout, * $P < 0.05$, ** $P < 0.01$, *** $P < 0.001$ unless otherwise stated.

RESULTS

PPC1 docetaxel- and radiation-derived PGCCs are not canonical stem cells

Radiation treatment failure or relapse after initial response to chemotherapy presents significant clinical challenges in prostate cancer patients. Most cancer treatment modalities target the mitotic process, with radiation inducing mitotic catastrophe and chemotherapeutic agents, such as docetaxel or cisplatin, promoting apoptosis. Therapy response varies between patients but can, in best case scenarios, eliminate the bulk of tumor cells to levels below clinical detection. However, even these patients may relapse, suggesting that a small residual fraction of malignant cells escaped therapy and formed a seed population that enabled the relapse. The goal of this study was to characterize cells that escape treatment. Here, we show that castration-resistant PPC1 prostate cancer cells that survive treatment with 5 nM docetaxel or 8 Gy of ionizing radiation are characterized by a large polyploid morphology (Fig. 1A). Despite the aberrant ploidy of these cells, they do not undergo mitotic catastrophe but, instead, reproduce through neosis, a process similar to budding with cellular extrusions carrying nuclei as shown in Fig. 1B. To determine whether these cells could be characterized as PGCCs as a consequence of endoreplication, we evaluated DNA content and cell size by flow cytometry. Results confirmed that the surviving population after treatment is highly enriched for G2+ cells, a population defined as having more than two full copies of genetic material. The polyploid cells were also measurably larger and more complex, as shown via forward scatter count (FSC) and side scatter count (SCC), respectively. The SCC measure was found to be sufficient to capture the PGCC population, with the G2+ population, scatter plot PGCCs, and high SCC cells all representing the same subset of cells (Fig. 1C, D; supplemental Fig. S2). We also used flow cytometry to determine whether PGCCs are enriched for stem cells that express CD133 and/or have increased ALDH activity (28). CD133 was not detected in any PPC1 sample (Fig. 1E, F), and ALDH activity remained stable after formation of PGCCs (Fig. 1G, H). Despite the lack of these stemness markers, PPC1 PGCCs were able to reestablish a mitotic population. Colonies derived from PGCCs typically present with a seed PGCC and a halo of small mitotic daughter cells (Fig. 1I)

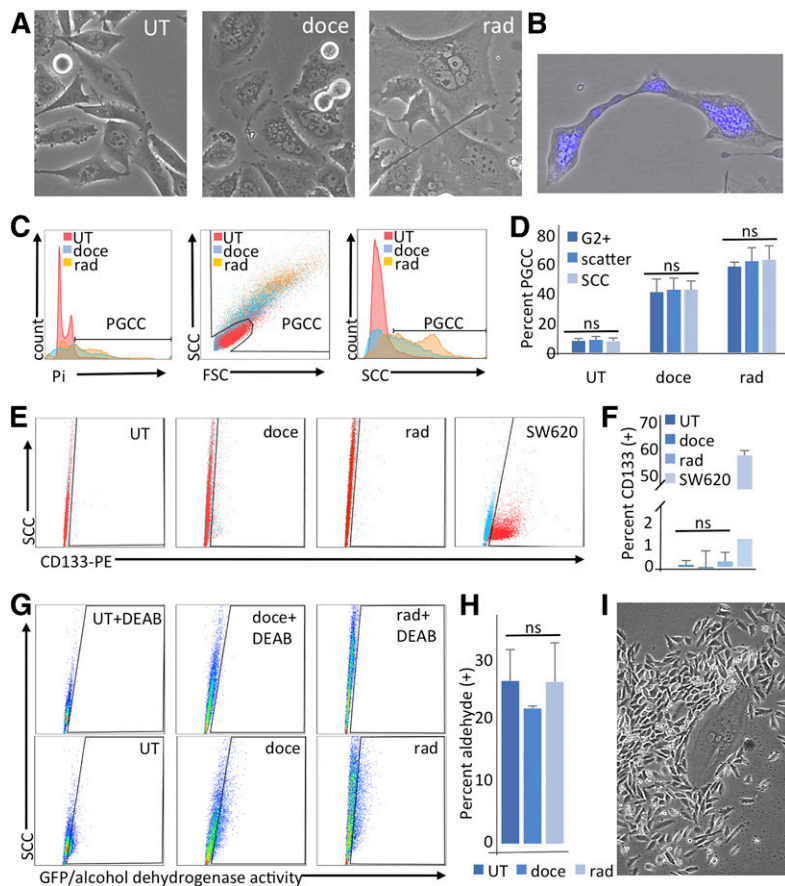


Fig. 1. Exposure to docetaxel or radiation induces polyploid morphology, but not canonical stemness markers in PPC1 cells. PPC1 cells were untreated (UT), treated with 5 nM docetaxel (doce), or exposed to 8 Gy radiation (rad). A: Treatments result in the formation of large multinuclear cells (PGCCs) within 48 h. B: An example of Hoechst-stained nuclei in polyploid PGCCs being shuttled during neosis. C: Characterization of PGCCs by flow cytometry 48 h after treatment using propidium iodide (Pi) staining to identify G2+ populations, SCC/FSC scatter plotting, or SCC alone. D: Quantification of C, $n = 4$. E: CD133 staining. Signals for unstained and anti-CD133-PE-stained PPC1 cells were overlaid. SW620 cells served as a positive control. F: Quantification of E, $n = 3$. G: Representative experiment of ALDH activity assay. Upper panels with DEAB serve as negative controls for lower panels. H: Quantification of ALDH activity assay ($n = 3$). I: A representative image of a PGCC-seeded colony surrounded by mitotic progeny after recovery from docetaxel treatment.

ASAHI is upregulated in PGCCs

ASAHI has been associated with therapy resistance in prostate cancer and is significantly elevated in patients who experience radiation treatment failure (19, 29). We hypothesized that ASAH1 would be necessary for escaping treatment stress. To test this hypothesis, we exposed cells to docetaxel or ionizing radiation and performed molecular analysis on cells that responded differently to the therapeutic stimulus. At 48 h, a significant portion of the culture appeared apoptotic and was collected as the “floating” fraction. The remaining attached population assumed PGCC morphology and was collected as the “adherent” fraction. Samples were then analyzed for differences in expression of sphingolipid metabolism enzymes. As shown in **Fig. 2A**, cleaved PARP indicating apoptosis was detected only in floating cells. In contrast, ASAH1 was detected only in the adherent population. Interestingly, expression of enzymes that function directly upstream (DES1) or downstream (SK1) of ASAH1 were not altered (Fig. 2A).

Next, we investigated the functional consequences of ASAH1 enrichment in the adherent cells and analyzed sphingolipids in apoptotic (ASAHI-null) and surviving (ASAHI-high) populations after exposure to docetaxel or radiation. In apoptotic cells that lack ASAH1 expression, total ceramides increased 2- to 3-fold, although the effect on individual ceramide species differed slightly (**Table 1**). C_{16} -ceramide increased most significantly with both radiation and docetaxel treatment (~ 2.5 -fold), while sphingosine was 2-fold lower in the floating compared with the

adherent population (Fig. 2B, C). Sphingosine serves as a substrate for SKs, which generate the pro-survival metabolite, SIP. However, despite changes in ceramides and sphingosine, SIP levels were not significantly altered between floating and adherent populations (Table 1).

We previously demonstrated that ceramide generated in response to radiation stress transcriptionally induces ASAH1 (19). To determine whether transcriptional activation of ASAH1 occurred in PGCCs, we generated a reporter plasmid in which GFP was expressed from the ASAH1 promoter. Analysis of adherent cells revealed that high levels of GFP are detected in approximately 50% of the cells (Fig. 2D, E). Docetaxel- and radiation-treated cells were gated to obtain two populations each: the high-SCC population that contains PGCCs and the high-GFP population that contains cells with activated ASAH1 promoters. When overlaid, these two populations were found to be overlapping but not fully concordant. Of interest, some PGCCs were not high-GFP (indicated by the red arrows in Fig. 2F). Fewer cells were high-GFP, but not identified as PGCCs (blue arrows in Fig. 2F). We concluded that the ASAH1 upregulation observed in Fig. 2A was primarily accounted for by PGCCs in the adherent population, and that this was fed at the transcriptional level. To rule out a genome-wide amplification of gene expression due to polyploidy, we measured DNA and RNA content in the treatment-resistant cells. DNA content was confirmed to be approximately 8-fold higher per cell after PGCC conversion, while RNA content was only about 2-fold higher (supplemental Fig. S3).

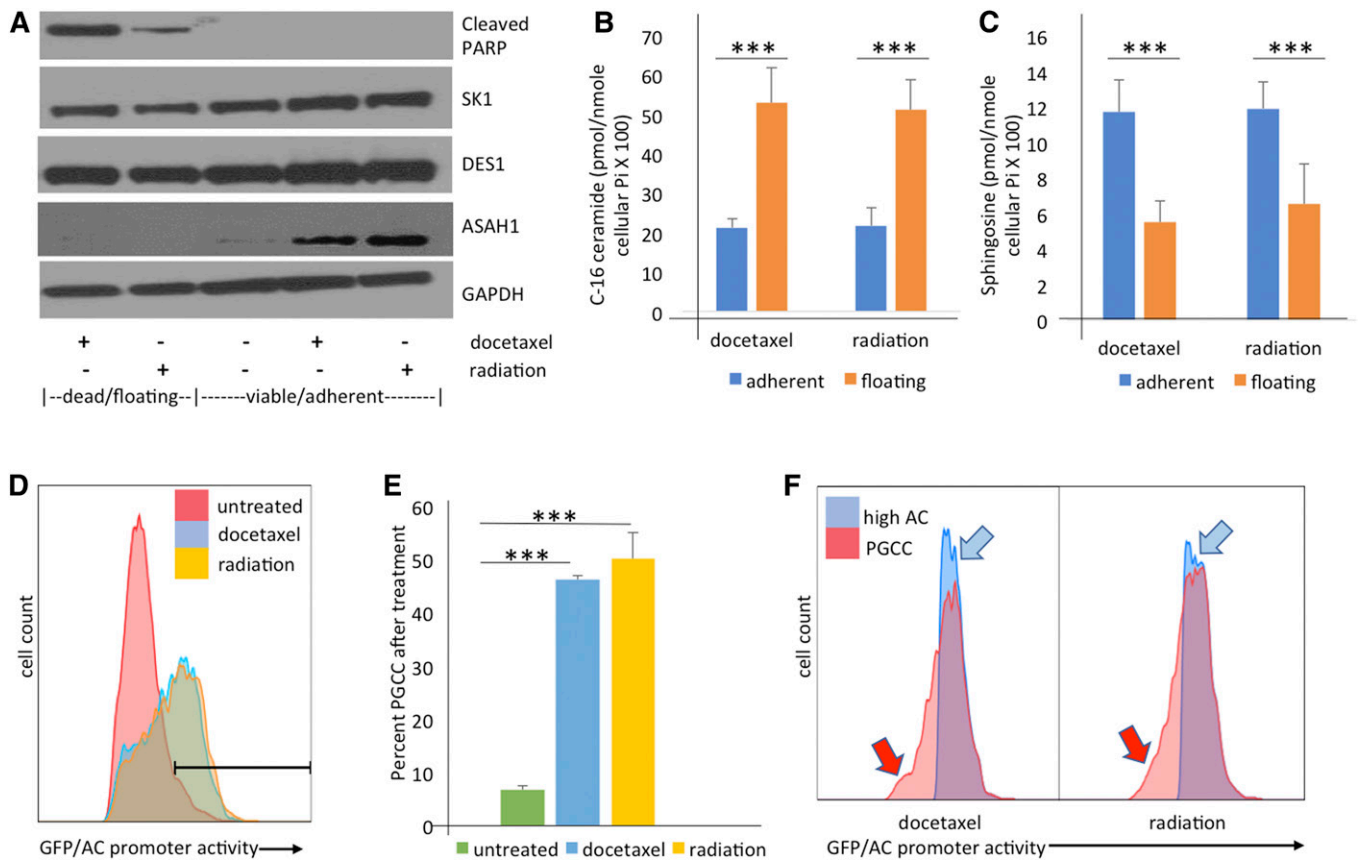


Fig. 2. PPC1 cells surviving chemotherapy or radiation upregulate ASAHI at the protein and transcriptional level. **A:** Western blot analysis comparing subpopulations after exposure to the indicated treatments, with floating/apoptotic cells analyzed separately from the adherent/resistant populations. Samples were analyzed for SK1, DES1, and ASAHI with GAPDH serving as loading control. **B, C:** Sphingolipid analysis of the floating/apoptotic cell subpopulation compared with the viable/adherent subpopulation. Data shown are from two representative experiments each performed in triplicate. $***P < 0.001$. **D:** Flow cytometric analysis of ASAHI promoter-driven GFP expression 48 h after exposure to 5 nM docetaxel or 8 Gy radiation. **E:** Quantification of **B**, shown as triplicate values representative of at least three independently performed experiments. **F:** Overlay of strongly positive GFP cells and the PGCC subpopulation in the same sample, demonstrating that the PGCCs account for the majority of the cells with high ASAHI promoter activity.

ASAH1 is not required for the formation of PGCCs

To further probe the role of ASAHI in PGCCs, we generated PPC1 cells that stably express an inducible shRNA-targeting ASAHI. ASAHI knockdown was confirmed by Western blot analysis, and lipidomics analysis was used to evaluate sphingolipid modulation (supplemental Fig. S4A–C). To test whether cells expressing ASAHI shRNA are able to form PGCCs, we exposed them to docetaxel and radiation. After 2 days of treatment, similar percentages of PGCCs were detected regardless of ASAHI expression, and cultures visually appeared the same, with loss of apoptotic cells and the formation of a robust monolayer of PGCCs (Fig. 3A). These results suggest that reduced expression of ASAHI does not affect the initial response of cells to therapy. Next, we confirmed the results obtained via genetic knockdown of ASAHI through pharmacological inhibition of ASAHI with LCL-521. LCL-521 is structurally based on the ASAHI inhibitor, B13, but is modified with *N,N*-dimethylglycine (DMG) esters to generate a pro-drug with lysosomotropic properties (25). Through lysosomal targeting, LCL-521 specifically affects ASAHI (supplemental Fig. S4D). Treatment of PPC1 cells with LCL-521 for 5 h

resulted in significantly reduced levels of sphingosine and an associated increase in ceramide (supplemental Fig. S4E, F). Interestingly, sphingosine levels rebounded within 24 h, while ceramide remained elevated (supplemental Fig. S4E, F). Similar to ASAHI shRNA, pharmacological inhibition of the enzyme with LCL-521 did not affect the formation of PGCCs (Fig. 3B).

ASAH1 is required for PGCC neosis in prostate cancer cells

It has been established that lack of ASAHI is embryonic lethal at the 2-cell stage (22), and recently Niu et al. (3) have elegantly described treatment-resistant PGCCs as the somatic equivalent of blastomeres at the 2- to 16-cell stage of embryogenesis. We hypothesized that ASAHI plays a parallel role in neosis of blastomeres and PGCCs. To test this hypothesis, we treated cells expressing nontargeting or ASAHI shRNAs with docetaxel or radiation to form PGCCs and then allowed those populations to recover. As shown in Fig. 4A, cells expressing the nontargeting (scrambled) shRNA were able to repopulate, with small cells filling in gaps between PGCCs, while lack of ASAHI expression

TABLE 1. Sphingolipid composition in PPC1 cells

Sphingolipid	Docetaxel		Radiation	
	Adherent [pmol SL/nmol Pi ($\times 100$)]	Floating [pmol SL/nmol Pi ($\times 100$)]	Adherent [pmol SL/nmol Pi ($\times 100$)]	Floating [pmol SL/nmol Pi ($\times 100$)]
C ₁₆ -ceramide	21.28 \pm 2.09	52.92 \pm 9.03 ^a	21.82 \pm 4.42	51.10 \pm 7.82 ^a
C ₂₂ -ceramide	26.12 \pm 10.13	78.98 \pm 8.38 ^a	27.72 \pm 17.08	71.24 \pm 24.90 ^b
C _{22:1} -ceramide	10.88 \pm 3.60	30.52 \pm 4.96 ^a	12.08 \pm 7.18	41.55 \pm 19.46 ^b
C ₂₄ -ceramide	139.32 \pm 25.97	352.35 \pm 27.71 ^a	147.66 \pm 71.10	274.27 \pm 114.44 ^b
C _{24:1} -ceramide	137.48 \pm 65.35	322.87 \pm 47.60 ^c	142.54 \pm 96.40	305.30 \pm 95.44 ^c
C ₂₆ -ceramide	23.51 \pm 1.85	53.49 \pm 9.30 ^a	20.61 \pm 7.13	25.47 \pm 12.78
C _{26:1} -ceramide	22.65 \pm 5.31	49.19 \pm 4.70 ^a	17.23 \pm 7.82	29.61 \pm 15.05
Other ceramides	12.73 \pm 3.07	24.24 \pm 8.57 ^b	14.37 \pm 0.69	27.51 \pm 15.22
dhC ₁₆ -ceramide	1.12 \pm 0.44	3.36 \pm 1.36	0.85 \pm 0.35	2.25 \pm 1.67
Sphingosine	11.67 \pm 1.84	5.49 \pm 1.16 ^a	11.87 \pm 1.52	6.52 \pm 2.30 ^c
SIP	0.21 \pm 0.05	0.21 \pm 0.03	0.30 \pm 0.06	0.40 \pm 0.16
Total ceramide	394.0 \pm 106.6	964.6 \pm 74.1 ^a	404.0 \pm 218.5	834.90 \pm 313.60 ^b

Cells were exposed to 5 nM docetaxel or 8 Gy radiation. After 48 h, floating and adherent cells were analyzed for sphingolipids using LC/MS. Data are the average and standard deviation from two independent experiments each performed in triplicate expressed as picomoles of sphingolipid (SL) per nanomole of inorganic phosphate (Pi) (pmol SL/nmol Pi) \times 100. Other ceramides represents the sum of C₁₄, C₁₈, C_{18:1}, C₂₀, C_{20:1}, and C_{20:4}.

^a $P < 0.0001$.

^b $P < 0.05$.

^c $P < 0.001$.

precluded this reproduction, leaving only scattered PGCCs. The arrested PGCCs expressing ASAH1 shRNA retained their polynuclear status, and also sprouted thin branching appendages, but appeared unable to successfully extrude nuclei for budding (Fig. 4A). We repeated the experiment using LCL-521 to pharmacologically inhibit ASAH1. Again, only PGCCs under control conditions were able to generate “neotic offspring,” whereas PGCCs in the presence of LCL-521 did not (Fig. 4B). Cellular morphology with pharmacological ASAH1 inhibition was similar to ASAH1 genetic knockout (Fig. 4B).

To further confirm the hypothesis that ASAH1 is required for neosis by PGCCs, we enriched PGCCs with a filtration step. Docetaxel- and radiation-induced PGCCs were generated, the surviving cells passed through a 20 micron filter, and cells retained by the filter were considered to be an enriched PGCC population. These cells were then sparsely and evenly replated, allowed to recover in the absence or presence of LCL-521, and PGCCs that successfully generated new colonies were counted. Colony formation in the presence of LCL-521 was significantly reduced in PGCCs generated in response to chemotherapy or radiation stress (Fig. 5A, B). These results support our hypothesis that LCL-521 functions as a neosis inhibitor.

Lung cancer cells are also dependent on ASAH1 for neosis

Although prostate cancer is the second most common cancer in males, the most deadly malignancy is lung cancer (30). Because neosis has been observed in lung cancer models (9), we were interested in determining whether ASAH1 also functioned as a neosis inhibitor in this cancer. For evaluation of LCL-521 in lung cancer, we selected A549, a non-small cell lung cancer (NSCLC) cell line. Compared with PPC1 cells, A549 cells express higher basal levels of ASAH1 (supplemental Fig. S5A). In the absence of treatment stress, exposure to 10 μ M LCL-521 did not

significantly affect viability (supplemental Fig. S5B). Exposure to LCL-521 for 5 h significantly decreased levels of sphingosine and increased ceramide (supplemental Fig. S5C, D). Because cisplatin is the clinically relevant drug for NSCLC, we used cisplatin rather than docetaxel as the chemotherapy stress in this model. Similar to PPC1 cells, exposure of A549 cells to radiation or chemotherapy resulted in the formation of multi-nucleated cells capable of undergoing neosis (supplemental Fig. S5E, F). Next, we repeated the filtration-based PGCC selection followed by the colony counting assay. Following therapy stress, only PGCCs in the control groups were able to undergo neosis, while treatment with 10 μ M LCL-521 nearly completely prevented recovery (Fig. 5C, D). Taken together, our results suggest that LCL-521 acts as a neosis inhibitor across cells derived from different cancers and multiple treatment modalities.

DISCUSSION

The parallels between embryogenesis and carcinogenesis have been explored in great detail, covering cell signaling, morphology, cell fate, and phenotypic markers (10, 31). One aspect of biology that has not been adequately considered from this viewpoint is the role of sphingolipid metabolism. Here, we explored the specific aspect of carcinogenesis inherent in posttreatment cancer relapse. Our group has been interested in how ASAH1 inhibition precludes relapse since observing that the ASAH1 inhibitor, LCL-521, could eliminate relapse in a radiation treatment xenograft model of prostate cancer (19). The finding was striking in its binary result: loss of ASAH1 function abrogated relapse entirely, rather than simply decreasing its frequency or severity. In this model, radiation alone or radiation combined with LCL-521 was used to treat PPC1 tumor xenografts, and all animals reached clinical remission. However, over the course of a 100 day follow-up study,

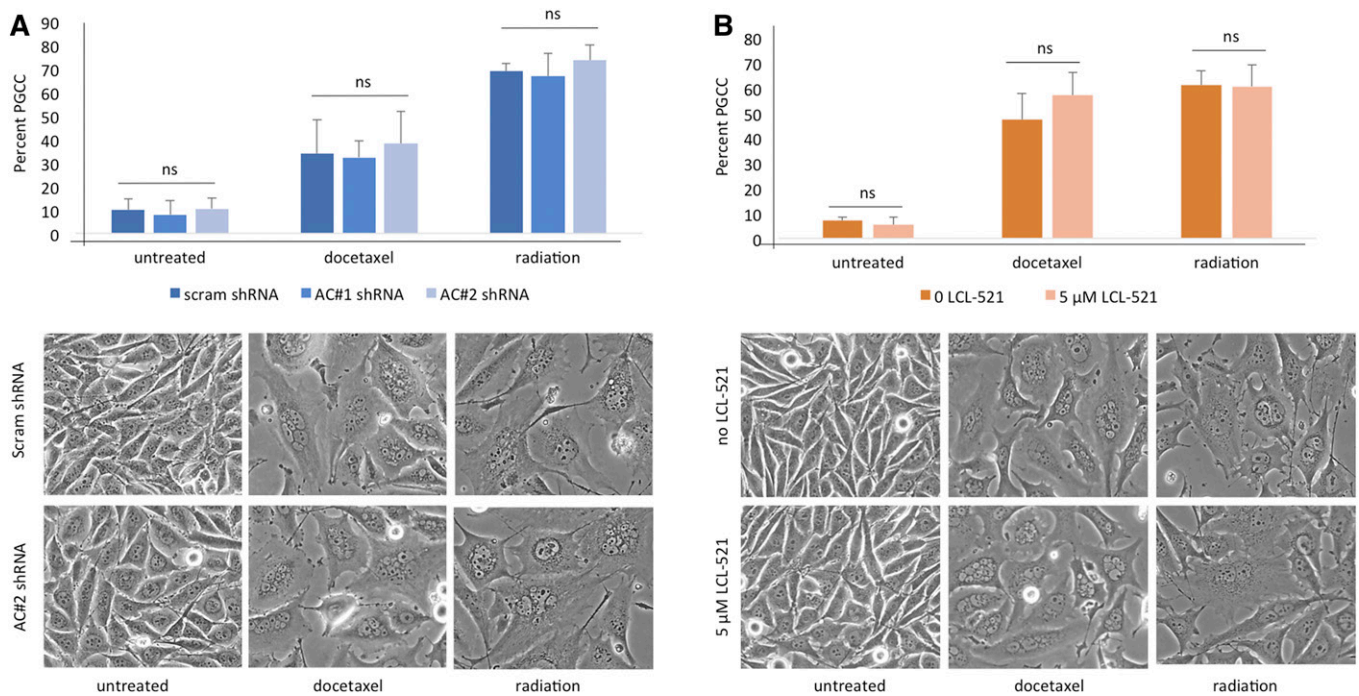


Fig. 3. Inhibition of ASAHI does not preclude the formation of PGCCs. **A:** Flow cytometry analysis (upper panel) and visual assessment (lower panel) of the PGCC population in PPC1 cells expressing scrambled shRNA or ASAHI-targeting shRNA. **B:** Flow cytometry analysis (upper panel) and visual assessment (lower panel) of the PGCC population in PPC1 cells treated with 5 μ M LCL-521. The graphs in A and B represent values from multiple independent experiments performed in replicates.

all animals treated with radiation alone robustly regrew tumors, while animals cotreated with radiation and LCL-521 showed no sign of tumor regrowth. This finding suggested that the appearance of remission in animals treated with only radiation actually included an undetectable population of resistant cells that could reestablish the cancer over time, whereas this unnamed population was inhibited or eliminated by LCL-521 treatment.

Based on observations in the current study, we postulated that the cell population capable of surviving treatment and later initiating relapse consists of PGCCs that are strictly dependent on ASAHI. PGCCs formed in both prostate cancer (PPC1) cells and NSCLC (A549) cells when exposed to their clinically relevant treatments of docetaxel/radiation or cisplatin/radiation, respectively. Analysis of the treatment-resistant PPC1-derived PGCCs revealed that ASAHI was upregulated relative to treatment-sensitive cells (Fig. 2A). Furthermore, PGCCs required ASAHI for neosis (Figs. 4, 5). The underlying mechanism for this dependence on ASAHI is of great interest. Previous studies have suggested that ASAHI-generated sphingosine can serve as substrate for SK1 in cancer cells to promote Akt-mediated signaling and the nuclear export of the tumor suppressor, PTEN (phosphatase and tensin homolog) (32, 33). However, PGCCs did not express elevated levels of SK1 and the SK product, SIP, a pro-survival lipid, increased compared with treatment-sensitive cells (Fig. 2A, Table 1). Intracellular sphingosine levels in adherent cells are higher than in cells that are dying. One possibility is that, in PGCCs, sphingosine has a different role than simply serving as an intermediary between ceramide

and SIP. A recent report showed that one biological target of sphingosine is cyclin-dependent kinase 1 (CDK1). Diril et al. (35) demonstrated that intracellular accumulation of sphingosine results in inactivation of CDK1, thereby pausing mitosis, whereas conversion of sphingosine to SIP strongly promoted mitosis (34). CDK1-deficient mouse hepatocytes are unable to divide, but can regenerate through endoreplication, which further supports a relationship between polyploidy and CDK1 (35). On the other hand, cells expressing ASAHI shRNA did not have reduced sphingosine levels compared with control shRNA, and pharmacological inhibition of ASAHI with LCL-521 only temporarily decreased sphingosine with levels rebounding by 24 h (supplemental Fig. S3). This suggests the possibility that other ceramidases compensate for reduced levels of sphingosine in the absence of ASAHI activity. In contrast, the increase in ceramide was maintained in cells lacking ASAHI and after 24 h of LCL-521 treatment, indicating the possibility that sustained elevated levels of ceramide are required to prevent neosis.

Our results demonstrate that the formation of PGCCs is ASAHI-independent (Fig. 3), but that neosis is ASAHI-dependent (Figs. 4, 5). The dependence of PGCCs on ASAHI fits seamlessly with the established idea of PGCCs being formed through a process of dedifferentiation to a blastomere-like state, which led to our working model that describes the parallel roles of ASAHI in embryonic development and cancer (Fig. 6). During embryonic development, lack of ASAHI does not interfere with the formation of zygotes, as an ASAHI-deficient egg and ASAHI-deficient sperm can fuse. However, the resulting zygote can only

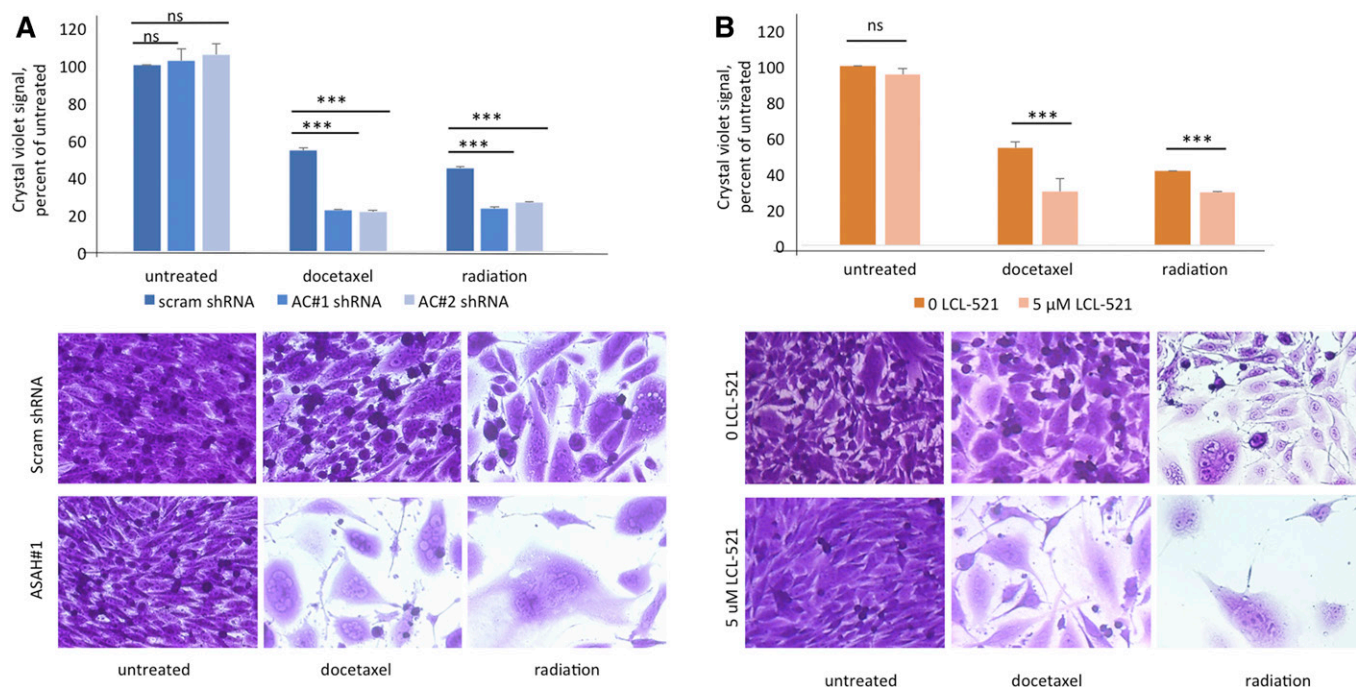


Fig. 4. Inhibition of ASAHI does arrest PGCCs and functions as a neosis inhibitor. A: PPC1 cells with scrambled or ASAHI-targeting shRNA were exposed to 5 nM docetaxel or 8 Gy radiation to form PGCCs. At 48 h, the PGCCs were allowed to recover followed by crystal violet staining with one triplicate set shown. B: PPC1 cells maintained in normal medium or in 5 μ M of LCL-521 were treated with 5 nM docetaxel or exposed to 8 Gy radiation to form PGCCs. Cultures were allowed to recover for 3–6 days, $n = 4$. Top panels represent quantification of staining ($***P < 0.001$) and bottom panels shows representative images.

perform cleavage once, reaching the 2-cell blastomere stage before ASAHI dependence becomes critical (22). Similarly, the formation PGCCs in response to mitotic poisons in cancer cells is ASAHI-independent, but regeneration via neosis is ASAHI-dependent.

PGCCs have been observed in a wide variety of cancers, including after treatment in relapsed cancer (2, 7, 10, 36–40). Certainly, they fit some of the functional definitions of stem cells, in that they survive treatment, divide asymmetrically, and are able to reestablish disease. A single PGCC can establish a tumor in animal models, suggesting that these cells have properties of CSCs (39). However, our experiments suggest that PGCCs may not be canonical stem cells, because known stem cell markers remain unchanged (Fig. 1E–H). Additional analysis will be required to determine the nature and possible markers of PGCCs. Other groups studying the biology of neosis have suggested that the PGCC stage may function as a warehouse for the next generation of cells, and that this new generation more closely matches the definition of CSCs (10, 12). These PGCC progeny, termed “Raju” cells, share transient CSC features (such as reactivation of telomerase and potential to differentiate) and are also worthy of focused attention as drivers of relapse. However, if neosis in PGCCs can be prevented through ASAHI inhibition, the threat of stem-like Raju cells could be addressed preemptively, thus preventing relapse.

A recent review suggested that the current treatment focus on inhibiting mitosis in cancer cells is only addressing part of the disease process. Without a tandem inhibition of neosis, cancer patients may be left with a posttreatment

occult subpopulation of dedifferentiated cancer cells that are less ordered and more dangerous than the original disease (8). It is widely understood that the biology of cancer relapse tends to be more aggressive, more metastatic, and more resistant to treatment, which has largely been attributed to the fact that the cells remaining after treatment have been selected for hardiness. Research in the neosis field suggests that the resistant cells are not only hardy, but, due to dedifferentiation and highly aberrant asymmetrical division of nuclear material, are in fact more genetically unstable (41).

Our data suggest that making ASAHI a priority target in cancer therapy could, for the first time, rationally address a mechanism that underlies relapse, which has immediate clinical applications. While ASAHI is a druggable target, specific inhibitors of this enzyme are still under development (29). However, two drugs that are in clinical use have been shown to inhibit ASAHI. Recently, the 5-fluorouracil derivative, capecitabine, was shown to directly bind to and inactivate ASAHI (42). Capecitabine has been used as an adjuvant chemotherapy in China, Japan, and Finland, but is not FDA-approved in the United States (43). Tamoxifen also inhibits ASAHI in cancer cells, although the mechanism appears to involve a decrease in ASAHI protein levels rather than direct enzymatic inhibition (44).

An alternate approach to targeting ASAHI is to identify other gene products for which full genetic ablation is embryonic lethal at the blastomere stage but largely phenotype-free in adult animals, which could lead to additional novel druggable targets to inhibit neosis. To date, research

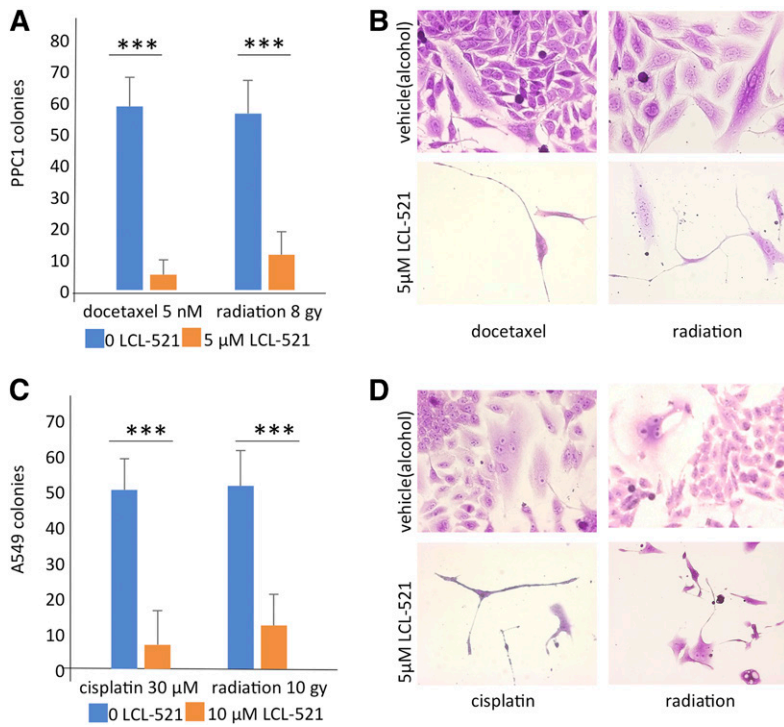



Fig. 5. ASAHI inhibition limits the formation of colonies from PGCCs in multiple cancer cell lines. **A:** PGCCs derived from PPC1 cells treated with docetaxel or radiation were captured via filtration, sparsely replated in the absence or presence of 5 μM LCL-521, and allowed to recover, $n = 3$ ($***P < 0.001$). **B:** Representative images of PGCC recovery from **A**. **C:** Colony formation assay of filtration-captured A549 PGCCs in the absence and presence of 10 μM LCL-521, $n = 3$ ($***P < 0.001$). **D:** Representative images of A549 PGCCs generating new colonies (top) or arresting (bottom).

on therapies that target neosis has been limited. One drug with possible anti-neotic effects is mifepristone. A recent study demonstrated that mifepristone, an antiprogesterin that is used as emergency contraception, inhibited the regrowth of a cisplatin-resistant A549 lung cancer cell subpopulation, which presumably reproduced via neosis (45). Interestingly, similar to LCL-521, mifepristone resulted in the formation of spindle-like cellular projections. Furthermore, like the inhibition of ASAHI, mifepristone would normally be considered toxic to early stages of development without dire consequences for differentiated cells. Although carmofur and tamoxifen inhibit ASAHI through “off-target” effects, it is not known whether mifepristone inhibits ASAHI or whether the drug inhibits a different target that is required for neosis. Neosis inhibitors have the potential to be used in conjunction with

radiation or chemotherapy to eliminate PGCCs, as they are generated due to therapy stress. Because neosis or neosis-like processes are limited to PGCC or embryonic development, such an approach would presumably have relatively few side effects.

In summary, parallels between embryogenesis and carcinogenesis have been elucidated with increasing levels of sophistication over decades. We were particularly interested in the connection between PGCCs and blastomeres (3). During development, blastomeres are not only dependent on ASAHI, but form the basis of the later stage trophoblasts, which also share characteristics with PGCCs, including a tendency toward polyploidy and dependence on ASAHI (2, 10, 22, 46). Our study presents actionable data that suggests a way to leverage these parallels into cancer treatment. Expression of ASAHI shRNA had very little phenotypic effect on PPC1 cells at baseline, and pharmacological inhibition of ASAHI inhibition was also largely ineffective against mitosis, because neither PPC1 prostate cancer cells nor A549 lung cancer cells were significantly impacted by exposure to LCL-521 alone. In contrast, once cancer cells were forced into a PGCC state to avoid mitotic poisons, inhibition of ASAHI resulted in dramatic loss of potential to undergo neosis. Therefore, combination of traditional mitosis-targeting treatments for bulk tumor reduction and ASAHI inhibition to prevent neosis in PGCCs may be the key to a robustly effective therapy. 

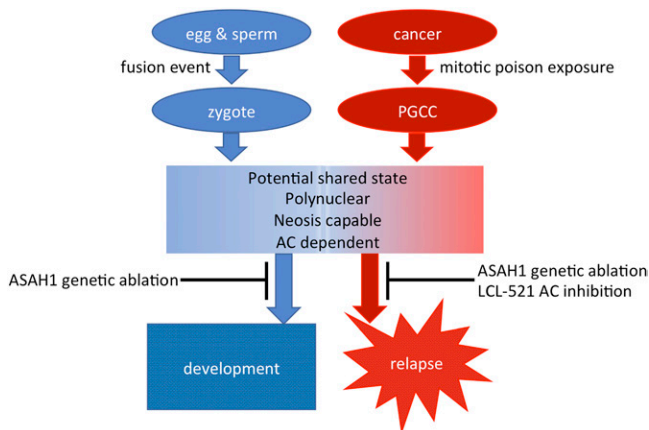


Fig. 6. A model of parallels between ASAHI during embryonic development and cancer therapy. For details please refer to the Discussion.

The authors thank Drs. Dean Tang, Marion Sewer, and Besim Ogetmen for sharing reagents and Ben Gilbertson for critical reading of the manuscript. The authors also thank the Lipidomics and Flow Cytometry Shared Resources for their excellent technical support. The Hollings Cancer Center shared resources are supported in part by P30 CA138313.

REFERENCES

- Schoenfelder, K. P., and D. T. Fox. 2015. The expanding implications of polyploidy. *J. Cell Biol.* **209**: 485–491.
- Edgar, B. A., and T. L. Orr-Weaver. 2001. Endoreplication cell cycles: more for less. *Cell.* **105**: 297–306.
- Niu, N., I. Mercado-Urbe, and J. Liu. 2017. Dedifferentiation into blastomere-like cancer stem cells via formation of polyploid giant cancer cells. *Oncogene.* **36**: 4887–4900.
- Liu, J. 2018. The dualistic origin of human tumors. *Semin. Cancer Biol.* **53**: 1–16.
- Illidge, T. M., M. S. Cragg, B. Fringes, P. Olive, and J. A. Erenpreisa. 2000. Polyploid giant cells provide a survival mechanism for p53 mutant cells after DNA damage. *Cell Biol. Int.* **24**: 621–633.
- Makarovsky, A. N., E. Siryaporn, D. C. Hixson, and W. Akerley. 2002. Survival of docetaxel-resistant prostate cancer cells in vitro depends on phenotype alterations and continuity of drug exposure. *Cell. Mol. Life Sci.* **59**: 1198–1211.
- Mittal, K., S. Donthamsetty, R. Kaur, C. Yang, M. V. Gupta, M. D. Reid, D. H. Choi, P. C. G. Rida, and R. Aneja. 2017. Multinucleated polyploidy drives resistance to docetaxel chemotherapy in prostate cancer. *Br. J. Cancer.* **116**: 1186–1194.
- Ogden, A., P. C. Rida, B. S. Knudsen, O. Kucuk, and R. Aneja. 2015. Docetaxel-induced polyploidization may underlie chemoresistance and disease relapse. *Cancer Lett.* **367**: 89–92.
- Puig, P. E., M. N. Guilly, A. Bouchot, N. Droin, D. Cathelin, F. Bouyer, L. Favier, F. Ghiringhelli, G. Kroemer, E. Solary, et al. 2008. Tumor cells can escape DNA-damaging cisplatin through DNA endoreduplication and reversible polyploidy. *Cell Biol. Int.* **32**: 1031–1043.
- Rajaraman, R., D. L. Guernsey, M. M. Rajaraman, and S. R. Rajaraman. 2006. Stem cells, senescence, neosis and self-renewal in cancer. *Cancer Cell Int.* **6**: 25.
- Rajaraman, R., M. M. Rajaraman, S. R. Rajaraman, and D. L. Guernsey. 2005. Neosis—a paradigm of self-renewal in cancer. *Cell Biol. Int.* **29**: 1084–1097.
- Sundaram, M., D. L. Guernsey, M. M. Rajaraman, and R. Rajaraman. 2004. Neosis: a novel type of cell division in cancer. *Cancer Biol. Ther.* **3**: 207–218.
- Leclerc, J., D. Garandeau, C. Pandiani, C. Gaudel, K. Bille, N. Nottet, V. Garcia, P. Colosetti, S. Pagnotta, P. Bahadoran, et al. 2019. Lysosomal acid ceramidase ASAH1 controls the transition between invasive and proliferative phenotype in melanoma cells. *Oncogene.* **38**: 1282–1295.
- Camacho, L., O. Meca-Cortes, J. L. Abad, S. Garcia, N. Rubio, A. Diaz, T. Celia-Terrassa, F. Cingolani, R. Bermudo, P. L. Fernandez, et al. 2013. Acid ceramidase as a therapeutic target in metastatic prostate cancer. *J. Lipid Res.* **54**: 1207–1220.
- Nguyen, H. S., S. Shabani, A. J. Awad, M. Kaushal, and N. Doan. 2018. Molecular markers of therapy-resistant glioblastoma and potential strategy to combat resistance. *Int. J. Mol. Sci.* **19**: E1765.
- Bai, A., C. Mao, R. W. Jenkins, Z. M. Szulc, A. Bielawska, and Y. A. Hannun. 2017. Anticancer actions of lysosomally targeted inhibitor, LCL521, of acid ceramidase. *PLoS One.* **12**: e0177805.
- Doan, N. B., H. Alhajala, M. M. Al-Gizawi, W. M. Mueller, S. D. Rand, J. M. Connelly, E. J. Cochran, C. R. Chitambar, P. Clark, J. Kuo, et al. 2017. Acid ceramidase and its inhibitors: a de novo drug target and a new class of drugs for killing glioblastoma cancer stem cells with high efficiency. *Oncotarget.* **8**: 112662–112674.
- Lai, M., N. Realini, M. La Ferla, I. Passalacqua, G. Matteoli, A. Ganesan, M. Pistello, C. M. Mazzanti, and D. Piomelli. 2017. Complete acid ceramidase ablation prevents cancer-initiating cell formation in melanoma cells. *Sci. Rep.* **7**: 7411.
- Cheng, J. C., A. Bai, T. H. Beckham, S. T. Marrison, C. L. Yount, K. Young, P. Lu, A. M. Bartlett, B. X. Wu, B. J. Keane, et al. 2013. Radiation-induced acid ceramidase confers prostate cancer resistance and tumor relapse. *J. Clin. Invest.* **123**: 4344–4358.
- Esmatabadi, M. J., B. Bakhshinejad, F. M. Motlagh, S. Babashah, and M. Sadeghizadeh. 2016. Therapeutic resistance and cancer recurrence mechanisms: unfolding the story of tumour coming back. *J. Biosci.* **41**: 497–506.
- Navolanic, P. M., S. M. Akula, and J. A. McCubrey. 2004. Neosis and its potential role in cancer development and chemoresistance. *Cancer Biol. Ther.* **3**: 219–220.
- Eliyahu, E., J. H. Park, N. Shtraizent, X. He, and E. H. Schuchman. 2007. Acid ceramidase is a novel factor required for early embryo survival. *FASEB J.* **21**: 1403–1409.
- Eliyahu, E., N. Shtraizent, R. Shalgi, and E. H. Schuchman. 2012. Construction of conditional acid ceramidase knockout mice and in vivo effects on oocyte development and fertility. *Cell. Physiol. Biochem.* **30**: 735–748.
- Lucki, N., and M. B. Sewer. 2009. The cAMP-responsive element binding protein (CREB) regulates the expression of acid ceramidase (ASAH1) in H295R human adrenocortical cells. *Biochim. Biophys. Acta.* **1791**: 706–713.
- Bai, A., Z. M. Szulc, J. Bielawski, J. S. Pierce, B. Rembiesa, S. Terzieva, C. Mao, R. Xu, B. Wu, C. J. Clarke, et al. 2014. Targeting (cellular) lysosomal acid ceramidase by B13: design, synthesis and evaluation of novel DMG-B13 ester prodrugs. *Bioorg. Med. Chem.* **22**: 6933–6944.
- Voelkel-Johnson, C., Y. A. Hannun, and A. El-Zawahry. 2005. Resistance to TRAIL is associated with defects in ceramide signaling that can be overcome by exogenous C6-ceramide without requiring down-regulation of cellular FLICE inhibitory protein. *Mol. Cancer Ther.* **4**: 1320–1327.
- Tirodkar, T. S., P. Lu, A. Bai, M. J. Scheffel, S. Gencer, E. Garrett-Mayer, A. Bielawska, B. Ogretmen, and C. Voelkel-Johnson. 2015. Expression of ceramide synthase 6 transcriptionally activates acid ceramidase in a c-Jun N-terminal kinase (JNK)-dependent manner. *J. Biol. Chem.* **290**: 13157–13167.
- Skvortsov, S., I. I. Skvortsova, D. G. Tang, and A. Dubrovska. 2018. Concise review: prostate cancer stem cells: current understanding. *Stem Cells.* **36**: 1457–1474.
- Voelkel-Johnson, C., J. S. Norris, and S. White-Gilbertson. 2018. Interdiction of sphingolipid metabolism revisited: focus on prostate cancer. *Adv. Cancer Res.* **140**: 265–293.
- Siegel, R. L., K. D. Miller, and A. Jemal. 2019. Cancer statistics, 2019. *CA Cancer J. Clin.* **69**: 7–34.
- Vinnitsky, V. 2014. The development of a malignant tumor is due to a desperate asexual self-cloning process in which cancer stem cells develop the ability to mimic the genetic program of germline cells. *Intrinsically Disord. Proteins.* **2**: e29997.
- Beckham, T. H., J. C. Cheng, P. Lu, S. T. Marrison, J. S. Norris, and X. Liu. 2013. Acid ceramidase promotes nuclear export of PTEN through sphingosine 1-phosphate mediated Akt signaling. *PLoS One.* **8**: e76593.
- Beckham, T. H., J. C. Cheng, P. Lu, Y. Shao, D. Troyer, R. Lance, S. T. Marrison, J. S. Norris, and X. Liu. 2013. Acid ceramidase induces sphingosine kinase 1/S1P receptor 2-mediated activation of oncogenic Akt signaling. *Oncogenesis.* **2**: e49.
- Andrieu, G., A. Ledoux, S. Branka, M. Bocquet, J. Gilhodes, T. Walzer, K. Kasahara, M. Inagaki, R. A. Sabbadini, O. Cuvillier, and A. Hatzoglou. 2017. Sphingosine 1-phosphate signaling through its receptor S1P5 promotes chromosome segregation and mitotic progression. *Sci. Signal.* **10**: eaah4007.
- Diril, M. K., C. K. Ratnacaram, V. C. Padmakumar, T. Du, M. Wasser, V. Coppola, L. Tassarollo, and P. Kaldis. 2012. Cyclin-dependent kinase 1 (Cdk1) is essential for cell division and suppression of DNA re-replication but not for liver regeneration. *Proc. Natl. Acad. Sci. USA.* **109**: 3826–3831.
- Zhang, D., X. Yang, Z. Yang, F. Fei, S. Li, J. Qu, M. Zhang, Y. Li, X. Zhang, and S. Zhang. 2017. Daughter cells and erythroid cells budding from PGCCs and their clinicopathological significances in colorectal cancer. *J. Cancer.* **8**: 469–478.
- Ly, H., Y. Shi, L. Zhang, D. Zhang, G. Liu, Z. Yang, Y. Li, F. Fei, and S. Zhang. 2014. Polyploid giant cancer cells with budding and the expression of cyclin E, S-phase kinase-associated protein 2, stathmin associated with the grading and metastasis in serous ovarian tumor. *BMC Cancer.* **14**: 576.
- Parekh, A., S. Das, S. Parida, C. K. Das, D. Dutta, S. K. Mallick, P. H. Wu, B. N. P. Kumar, R. Bharti, G. Dey, et al. 2018. Multi-nucleated cells use ROS to induce breast cancer chemo-resistance in vitro and in vivo. *Oncogene.* **37**: 4546–4561.
- Zhang, S., I. Mercado-Urbe, Z. Xing, B. Sun, J. Kuang, and J. Liu. 2014. Generation of cancer stem-like cells through the formation of polyploid giant cancer cells. *Oncogene.* **33**: 116–128.
- Mirzayans, R., B. Andrais, and D. Murray. 2018. Roles of polyploid/multinucleated giant cancer cells in metastasis and disease relapse following anticancer treatment. *Cancers (Basel).* **10**: E118.
- Niu, N., J. Zhang, N. Zhang, I. Mercado-Urbe, F. Tao, Z. Han, S. Pathak, A. S. Multani, J. Kuang, J. Yao, et al. 2016. Linking genomic reorganization to tumor initiation via the giant cell cycle. *Oncogenesis.* **5**: e281.
- Dementiev, A., A. Joachimiak, H. Nguyen, A. Gorelik, K. Illes, S. Shabani, M. Gelsomino, E. E. Ahn, B. Nagar, and N. Doan.

- Molecular mechanism of inhibition of acid ceramidase by carmofur. *J. Med. Chem.* Epub ahead of print. December 7, 2018; doi:10.1021/acs.jmedchem.8b01723.
43. Sakamoto, J., K. Oba, T. Matsui, and M. Kobayashi. 2006. Efficacy of oral anticancer agents for colorectal cancer. *Dis. Colon Rectum.* **49**: S82–S91.
44. Morad, S. A., J. C. Levin, S. F. Tan, T. E. Fox, D. J. Feith, and M. C. Cabot. 2013. Novel off-target effect of tamoxifen—inhibition of acid ceramidase activity in cancer cells. *Biochim. Biophys. Acta.* **1831**: 1657–1664.
45. Kapperman, H. E., A. A. Goyeneche, and C. M. Telleria. 2018. Mifepristone inhibits non-small cell lung carcinoma cellular escape from DNA damaging cisplatin. *Cancer Cell Int.* **18**: 185.
46. Payne, S. G., D. N. Brindley, and L. J. Guilbert. 1999. Epidermal growth factor inhibits ceramide-induced apoptosis and lowers ceramide levels in primary placental trophoblasts. *J. Cell. Physiol.* **180**: 263–270.